IEEE Access
Multidisciplinary | Rapid Review | Open Access Journal

Received 4 February 2023, accepted 27 February 2023, date of publication 10 March 2023, date of current version 21 March 2023.

Digital Object Identifier 10.1109/ACCESS.2023.3255418

RESEARCH ARTICLE

Active Vibration Control Strategy for Online Application in a Range Extender

ZHANG JINYU[1], HU SONG[2,3], JU LONGYU[4], AND YANG FUYUAN[1]

[1]School of Vehicle and Mobility, Tsinghua University, Beijing 100084, China
[2]School of Mechanical Engineering, University of Science and Technology at Beijing, Beijing 100084, China
[3]Shunde Innovation School, University of Science and Technology Beijing, Foshan 528399, China
[4]Jing-Jin Electric Technologies Company Ltd., Beijing 100084, China

Corresponding authors: Yang Fuyuan (fyyang@mail.tsinghua.edu.cn) and Hu Song (husong_90@163.com)

This work was supported by Weichai Power Company Ltd., under Contract WCDL-GH-2022-0234.

ABSTRACT Noise, vibration and harshness are a big issue for hybrid vehicles especially in range extenders. Traditional vibration control and active damping control are generally used for suppressing vibration. Compared with traditional vibration control, active damping control is more flexible and effective in suppressing vibration. The basic idea of active damping control is controlling electric motor compensating for the torque of engine and reducing the vibration from the source. The reduction of vibration is highly depended on the compensation torque of the electric motor. A differently designed compensation torque has a significant impact on the active damping control effect. In this paper, an active damping control method for online application is proposed. And several kinds of compensation torque are designed for this method. Experiments on vibration performance are conducted to compare the effect of different compensation torque design in reducing vibration. And the results show that the compensation torque in the shape of square wave has potential for reducing vibration in all directions. Finally, a guiding tool for compensation design is proposed by correlation analysis and the relationship between designing factors and vibration is revealed.

INDEX TERMS Hybrid electric vehicles, range extender, active damping control, vibration control.

I. INTRODUCTION

Range extenders are a practicable option for replacing conventional vehicles due to its potential to save energy and lower emissions [1], [2]. A range extender usually comprises an internal combustion engine, an integrated starter generator (ISG), a driving motor and battery package, etc. The combination of the internal combustion engine and ISG motor is usually called the auxiliary power unit (APU). However, range extenders also have noise vibration and harshness (NVH) problems like the other hybrid vehicles [3], [4]. Research shows that vibration excited by APU is the crucial vibration issue of a range extender hybrid vehicle [4], [5]. Vibration problems will affect the life of components, the driving experience, and cause noise. Therefore, research on the vibration performance of the range extender and methods to improve its vibration performance is of great significance.

The associate editor coordinating the review of this manuscript and approving it for publication was Turgay Celik.

There are generally two types of vibration control: 1) traditional vibration control, which controls vibration passively through mechanical design, and 2) active vibration control, which actively reduces vibration from the source. Traditional vibration control like adding extra weight onto the crank arm [6], utilizing a dual-mass flywheel [7] or a special-structure engine [8] is still one of the most effective ways to improve vibration performance and it is widely used in vehicles. However, hybrid technology has brought more challenges to traditional vibration control. Firstly, the relatively constant parameters of the mechanical structure find it difficult to cope with the changing operating conditions of hybrid vehicles. Secondly, extra energy consumption will be generated with extra added weight. Furthermore, vibration characteristics are more complex for hybrid vehicles. Active vibration control is an alternative method to actively suppress vibration by utilizing the electric motor. The quick response of electric motor in a hybrid vehicle has brought a new possibility of achieving active vibration control.

Hence, active vibration control for hybrid vehicles has attracted more attention from researchers. The basic idea of active vibration control is quite simple. When the engine outputs a certain torque with fluctuation, the electric motor will output an extra torque with the opposite phase. As a result, the excitation of vibration caused by the internal combustion engine will become closer to a constant value. And the vibration and speed fluctuation can be reduced from the source.

Active vibration control was called active flywheel technology at first. The target of an active flywheel is reducing the speed fluctuation caused by the engine's torque, especially during the idling phase. The active flywheel was first proposed by Gusev et al. in 1997, whose simulation results showed its effectiveness for reducing vibration [9]. Then the concept was developed by Zaremlba et al. [10] based on learning control. And this algorithm was finally validated by experiments on a diesel engine [11]. Similar research had been carried out with a harmonic activation neural network by Beuschel [12]. However, the effect of active flywheel technology of early researches is generally limited by the maximum power of the electric motor and power loss of the electric motor.

With a more powerful electric motor being used in hybrid vehicles, the application of active damping control has expanded. And better performance in reducing vibration has been achieved. Then active damping control was used in a hybrid vehicle by Honda R&D Co., Ltd [13], and it was renamed the Integrated Motor Assist (IMA) system. The IMA system could suppress idle vibration by 3dB∼5dB. The Ford Motor Co. also achieved this technology by adaptive Proportion-Integration-Differentiation (PID) control [14]. A 65% reduction of idle speed fluctuation was achieved.

With the popularity of power-split hybrid electric vehicles, more researches focused on suppressing vibration caused by the complex structure. The representative research was completed by Toyota [15], [16]. This research mainly focused on vibration control during the start/stop process. The experimental results showed that about 60% of peak floor vibration is reduced and passengers should barely detect engine startup. Active damping control was also applied in the Ford Escape Hybrid [17]. Simulation and experiment results showed that active damping control was able to suppress driveline vibration effectively even with increased motor/generator disturbances and change in driveline stiffness. The Chrysler research group also achieved active damping control for power-split configuration via slide mode control [18]. Similar researches [17], [20], [21] using torque observer have also achieved good effects. Nowadays, vibration suppression of power-split configuration during start/stop can be effectively solved by active damping control [19].

However, the configuration of a range extender is quite different from the power-split configuration. The electric motor of a range extender is generally coaxial to the engine. Research [22], [23], and [24] mainly focuses on vibration control during the start/stop process in a range extender. Simulation results show that peak to peak force is reduced by about 31.2% by using active damping control. The difficulty is how to make an active damping control for online application. Hence, time delay of the communication system and mechanical response should be taken into consideration. Active torsional vibration control based on mode prediction was conducted by Chen [25] to cope with the time delay. Simulation results showed that torsional vibration was reduced by more than 90%. Jiang [26] researched a similar mode predictive control, and simulation results showed that acceleration oscillation was reduced about 80%. However, neither of these papers conducted experiments to verify the results. Meng's research is based on a torque fluctuation estimation and the vibration acceleration was reduced by about 8.4%∼11.1% [27].

The above studies have one thing in common. That is, the control target is how to make the compensation torque of the electric motor be more similar to the real engine ripple torque but with opposite phase. However, some researches about active damping control with the compensation torque in the shape of a square wave have been done. The vibration control during the startup process is illustrated in one study [28] and the effect of idle vibration reduction is illustrated in a paper [29]. By using a square waveform as compensation torque, the idle speed fluctuation is reduced by 79.2% and the vibration index proposed in [29] is reduced by 83%. More research on the steady state has been conducted [30]. Experimental results show that active damping control is effective over low speed and load ranges. Not only is the vibration performance enhanced, combustion stability and cylinder-by-cylinder uniformity are also improved by active damping control [31]. The waveform of compensation used in literature [28], [29], [30], [31] is the square waveform instead of being similar to the real engine ripple torque but with opposite phase.

Theoretically, the compensation torque with opposite phase of engine torque (which is called as the ideal waveform in the rest of this paper) is the optimal waveform for active damping control. However, considering the conversion of analog-to-digital signals and the time delay of motor response, the real compensation torque waveform tends to be deformed greatly. Hence the ideal waveform may not be the optimal waveform anymore. It is meaningful and necessary to find out what kind of waveform is more suitable for active damping control. and other kinds of waveforms (such as a square waveform and a pulse width modulation waveform) have to be taken into consideration. However, the problem is that none of these papers [28], [29], [30], [31] have compared the effect of active damping control with compensation torque in the shape of the square waveform and the ideal waveform. And the vibration indicators which is used to evaluate vibration performance are not directly getting from sensors. Hence, the question of which kind of compensation design is more suitable for online application is yet to be answered.

In this paper, an active damping control algorithm based on transient speed observer is proposed at first. And several kinds of waveforms including the ideal waveform, the square waveform and the PWM wave are designed for the proposed method. Experiments about which kind of compensation design is more suitable for embedded systems to actively suppress the vibration are conducted.

The contribution of this paper is summarized as follows:

1) A novel way of achieving active damping control for online application is proposed. Vibration acceleration was reduced by 52.50% at most in our experiments while the reduction of traditional vibration control is within 15%.

2) The influence of different kinds of waveforms is compared in this paper through experiments and the reasons for the difference are analyzed from the perspective of the frequency spectrum.

3) The relationship between design factors and vibration performance is revealed through correlation analysis.

II. ACTIVE DAMPING CONTROL AND DESIGN OF THE TRANSIENT SPEED OBSERVER

The basic idea of active damping control is quite simple. When the engine outputs a certain torque with fluctuation, the ISG (Integrated Starter and Generator) motor will output a torque with the opposite phase of the engine's ripple torque. And the result is that the whole output torque will be smoother and the rotational speed fluctuation will be smaller as well.

This section will introduce details of active damping control including an explanation of active damping control, modeling of the range extender and establishment of the transient speed observer.

A. ACTIVE DAMPING CONTROL

Configuration of the range extender researched in this paper is shown in Fig.1. The vibration control mainly focuses on controlling the vibration of the APU. The integrated starter generator (ISG) motor is directly coupled to the engine crankshaft. However, unlike a normal range extender, the rotor of the ISG motor is manufactured to replace the flywheel on the end of the crankshaft (as shown in Fig.2). Using this kind of technology will make the structure of the whole powertrain more compact and reduce the total cost. However, the problem is that the inertia of the rotor is generally smaller than that of the flywheel and the speed fluctuation and vibration will be enlarged with the decreasing inertia. Hence it is necessary to use active damping control to reduce the speed fluctuation and suppress the vibration.

The whole control scheme for online active damping control is shown in Fig.3. There are three parts of active damping control: (1) compensation torque feedforward control; (2) crank position real-time calculation; and (3) transient speed observer. The whole active damping control algorithm is programmed in the motor control unit (MCU).

Compensation torque feedforward control is used for calculating the compensation torque through a crank angle-torque look-up table. The main function of this part is to

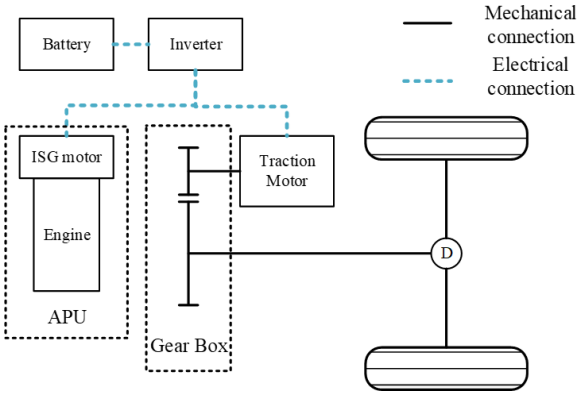

FIGURE 1. Configuration of range extender.

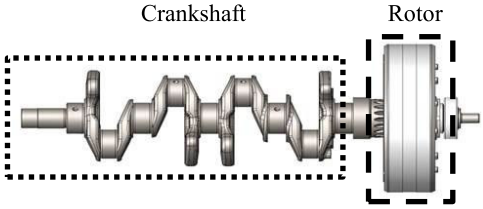

FIGURE 2. Structure of crankshaft and ISG rotor.

make the compensation torque get close to the target quickly and make active damping control suitable for real-time online application. Considering the working process of an internal combustion engine, it is easy to know that the transient torque of the engine is periodic and highly related to the crank angle. Hence, by calibrating the crank angle-torque look-up table offline, this part can be accomplished offline.

The real-time absolute position of the crankshaft needs to be provided for calculating the compensation torque. This information is generally provided for the engine control unit (ECU) not the MCU. However, active damping control algorithm is programmed into the MCU. Thereby, it is necessary to establish a method to provide that information. Crank position real-time calculation is used for this purpose. Except for the reason described above, crank position real-time calculation is also necessary to output the correct crank angle. Details of how crank position real-time calculation works and verification of its accuracy have been researched in a paper [30]. And crank position real-time calculation is directly used in this paper.

The control target of active damping control is reducing speed fluctuation as well as vibration. Hence, the value of the speed fluctuation range needs to be calculated. However, only average speed is provided for the ECU or MCU. In addition, conventional rotational speed measurement used in hybrid vehicles is unable to provide accurate information about the speed fluctuation range. In the end, a transient speed observer is established to provide accurate information.

The working principle of active damping control is as follows. The control target is the range of speed fluctuation. Through active damping control, the real value of the speed

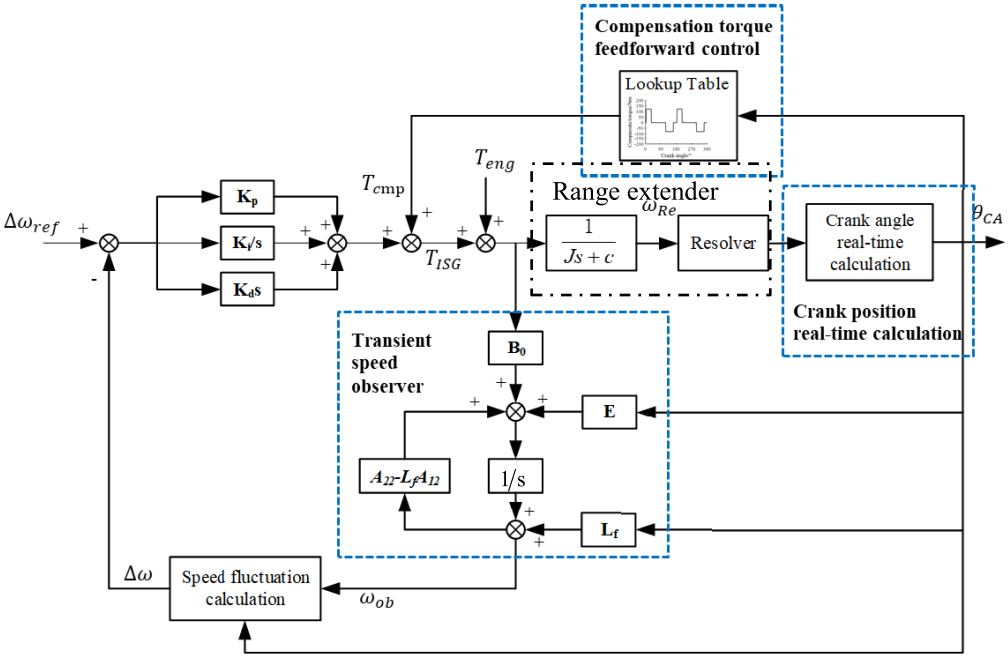

FIGURE 3. Control scheme of active damping control.

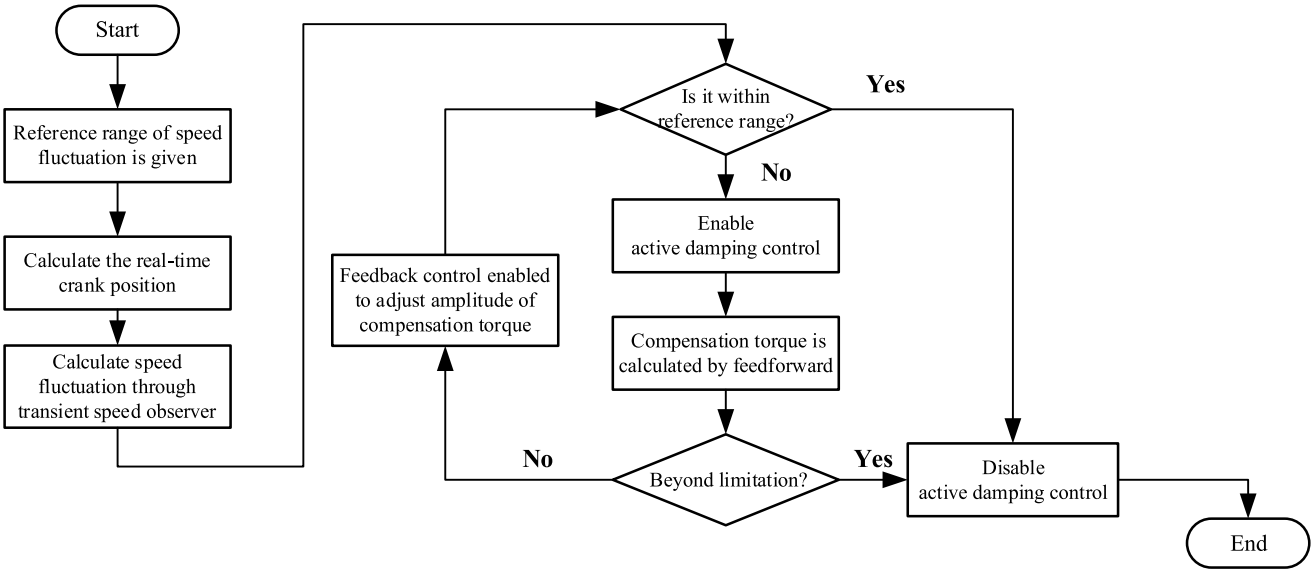

FIGURE 4. Flow chart of active damping control.

fluctuation range needs to be smaller than the reference value. This target is achieved by the ISG motor outputting extra compensation torque with appropriate amplitude and correct phase. The appropriate amplitude is guaranteed by the feedforward control with look-up table and feedback control with transient speed observer. The correct phase is guaranteed by crank position real-time calculation.

The working process of active damping control is shown in Fig.4.

Step 1: a reference value of speed fluctuation range is given.

Step 2: crank position real-time calculation method provides correct absolute position of the crankshaft.

Step 3: transient speed observer is used to calculate the real speed fluctuation range and then the real value is compared with the reference value.

Step 4: if the real value of speed fluctuation range is bigger than the reference value, active damping control is enabled.

And compensation torque is calculated through feedforward control and feedback control.

Step 5: if the real value of speed fluctuation range is still bigger than the reference value, repeat step 4 and enlarge the amplitude of compensation torque (actually, this process is accomplished by feedback automatically).

Step 6: if the real value of speed fluctuation range is smaller than the reference value, then the whole control process is completed. And active damping control will be disabled when there is no need to use it.

B. DYNAMIC MODEL FOR RANGE EXTENDER

The essential parts of active damping control have been described in section A above. This part focuses on establishing the transient speed observer. The next part discusses designing the compensation torque waveform.

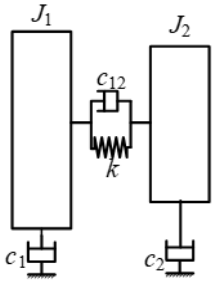

FIGURE 5. A dual-lumped-mass model.

Before establishing the transient speed observer, the range extender needs to be modeled, as shown in Fig.5. A dual-lumped-mass model is used to calculate the dynamic performance of the range extender.

$$T_{eng} = J_1\ddot{\theta}_1 + c_1\dot{\theta}_1 + k(\theta_1 - \theta_2) + c_{12}(\theta_1 - \theta_2) + T_{f1} \quad (1)$$

$$T_{ISG} = J_2\ddot{\theta}_2 + c_2\dot{\theta}_2 - k(\theta_1 - \theta_2) - c_{12}(\theta_1 - \theta_2) + T_{f2} \quad (2)$$

where, θ_1 is the rotational angle of the engine and θ_2 is the rotational angle of the ISG motor. T_{eng} is the transient torque of the engine. T_{ISG} is the transient torque of the ISG motor. J_1 is the inertia of the engine. J_2 is the inertia of the ISG motor. c_1 is the damping of the engine. c_2 is the damping of the ISG motor. k is the stiffness of the shaft and c_{12} is the damping of the shaft. Only output speed ($\dot{\theta}_2$) needs to be controlled. Hence, equation (1) and equation (2) are added together as:

$$T_{eng} + T_{ISG} = (J_1\ddot{\theta}_1 + J_2\ddot{\theta}_2) + (c_1\dot{\theta}_1 + c_2\dot{\theta}_2) + (T_{f1} + T_{f2}) \quad (3)$$

And let $\theta_1 = \theta_2$. The stiffness of this kind of structure is generally big because the rotor of the ISG motor is directly coupled to the crankshaft. Hence, the error between the rotational angle of the engine and the rotational angle of the ISG motor is generally small. Hence, it is reasonable to let $\theta_1 = \theta_2$.

The state space equation used for establishing the transient speed observer is finished.

$$\begin{cases} \dot{x}_1 = x_2 = \dot{\theta} \\ \dot{x}_2 = \frac{-(c_1+c_2)x_2 - (T_{f1}+T_{f2}) + (T_{eng}+T_{ISG})}{(J_1+J_2)} \end{cases} \quad (4)$$

where x_1 is the rotational angle. x_2 is the rotational speed. Now the question is how to calculate the torque of the engine.

The establishment of the engine's torque model is described as below. And the model is established using pressure signals of sensors installed on each cylinder and parameters of the crank mechanism.

When only considering one cylinder with a crank mechanism, the displacement x, velocity v, acceleration j of the piston can be obtained as follows:

$$x = h_{max} - rcos\varphi - \sqrt{l^2 - (rsin\varphi - d + e)^2} \quad (5)$$

$$\begin{aligned} v &= \frac{dx}{dt} = \frac{dx}{d\varphi}\frac{d\varphi}{dt} = \omega\frac{dx}{d\varphi} \\ &= \omega r[sin\varphi + \frac{(rsin\varphi - d + e)cos\varphi}{\sqrt{l^2 - (rsin\varphi - d + e)^2}}] \end{aligned} \quad (6)$$

$$\begin{aligned} j &= \frac{dv}{dt} = \frac{dv}{d\varphi}\frac{d\varphi}{dt} = \omega\frac{dv}{d\varphi} \\ &= \omega^2 r \left\{ cos\varphi + \frac{rcos2\varphi + (d-e)sin\varphi}{\sqrt{l^2 - (rsin\varphi - d + e)^2}} \right. \\ &+ [rsin\varphi cos\varphi - dcos\varphi + ecos\varphi] \\ &\left. \cdot \frac{(rsin\varphi - d + e)\, rcos\varphi}{\left[l^2 - (rsin\varphi - d + e)^2\right]^{\frac{3}{2}}} \right\} \end{aligned} \quad (7)$$

where h_{max} is the maximum stroke of the piston; r is crank radius; l is the center distance of the connecting rods; d is the offset distance of the crankshaft; e is the offset distance of the piston pin; φ is the angle of the crank (in addition, $\varphi = \theta$. But, in order to remove any confusion, they are written in a different format); and ω is angular velocity.

The pumping force, F_{gas}, caused by the variation of the cylinder pressure can be calculated as:

$$F_{gas} = \frac{\pi D^2}{4}(p_{gas} - p_0) \quad (8)$$

where p_{gas} is the pressure in the cylinder, p_0 is the pressure in the crankcase, and D is the cylinder bore.

The inertial force can be divided into two parts: rotational inertial force, F_r and reciprocating inertial force F_j.

Rotational inertial force, F_r, can be expressed as:

$$F_r = (m_q + m_b)\omega^2 r \quad (9)$$

where m_q is the equivalent mass of the bell crank and m_b is the equivalent mass of the connecting rod.

Reciprocating inertial force, F_j, can be expressed as:

$$F_j = -(m_p + m_a)j \quad (10)$$

where m_p is the equivalent mass of the piston and m_a is the other equivalent mass of the connecting rod.

The indicated torque of one cylinder can be calculated by the pumping force and reciprocating inertial force:

$$T_i = \frac{(F_{gas} + F_j) \cdot r \cdot \sin(\phi + \beta)}{\cos \beta} \tag{11}$$

where, T_i is the indicated torque of one cylinder, β is the swing angle of the connecting rod. And the relationship between β and ϕ is as follows:

$$l \sin \beta - e = r \sin \theta - d \tag{12}$$

An inline four-cylinder engine consists of four crank mechanisms, hence the indicated engine torque should be:

$$T_{eng} = \sum_{i=1}^{4} (T_i) \tag{13}$$

The calculation process needs to know the value of the transient speed of the engine. However, the speed fluctuation value is relatively smaller compared to the average speed value. Hence, ω can be replaced by average speed. This is important for establishing the transient speed observer.

C. TRANSIENT SPEED OBSERVER

Equation (4) can be rewritten into equation (14):

$$\begin{cases} \dot{x}_1 = x_2 = \dot{\theta} \\ \dot{x}_2 = \frac{-T_f + (T_{eng} + T_{ISG})}{J} \\ y = x_1 \\ T_f = T_{f1} + T_{f2} + c_1(\dot{\theta}_1 - \dot{\theta}_2) + c_2(\dot{\theta}_1 - \dot{\theta}_2) \end{cases} \tag{14}$$

where, T_f is the total damping force and it is related to the rotational speed. J is the total inertia. y is the output. In this paper, the output is the crank angle.

Equation (14) is highly non-linear because of the existence of T_f and T_{eng}. However, simplification has been made by treating them as a part of the input and equation (14) can be rewritten into:

$$\begin{cases} \dot{x}_1 = x_2 \\ \dot{x}_2 = k \cdot u \\ y = x_1 \end{cases} \tag{15}$$

where,

$$\begin{cases} u = -T_f + (T_{eng} + T_{ISG}) \\ k = \frac{1}{J} \end{cases} \tag{16}$$

Then the problem is simple to solve. The torque of the engine can be calculated (with the model established in the previous section) before calculating transient speed. And average speed can replace transient speed in calculating the torque of the engine. Hence, this method is practical online with the ECU providing average speed information.

However, if equation (15) is directly used for estimating transient speed, then the error between estimated value and real value would be large because of simplification. The estimated state space equation should be as follows:

$$\begin{cases} \dot{\hat{x}}_1 = A_{11}\hat{x}_1 + A_{12}\hat{x}_2 + B_1 u \\ \dot{\hat{x}}_2 = A_{21}\hat{x}_1 + A_{22}\hat{x}_2 + B_2 u \\ \hat{y} = \hat{x}_1 \end{cases} \tag{17}$$

where, $\hat{x}_1$ is the estimated value of rotational angle. $\hat{x}_2$ is the estimated value of rotational speed. y is the output. And $A_{11} = 0, A_{12} = 1, A_{21} = 0, A_{22} = 0, B_1 = 0, B_2 = k$.

Hence, feedback is needed to decrease or even eliminate the error. Luckily, the accurate crank angle (i.e. x_1) can be acquired by the crank position real-time calculation method. Thereby, a Luenberger reduced-order observer can be established.

Let $v = A_{21}y + B_2 u$, $z = A_{12}\hat{x}_2 = \dot{y} - A_{11}y - B_1 u$, then equation (17) will be rewritten into equation (18):

$$\begin{cases} \dot{\hat{x}}_2 = A_{22}\hat{x}_2 + v \\ z = A_{12}\hat{x}_2 \end{cases} \tag{18}$$

Now the system expressed by equation (17) is transformed into a new linear constant system expressed by equation (18). Considering output feedback control $L_F z$.

$$\begin{cases} \dot{\hat{x}}_2 = (A_{22} - L_f A_{12})\hat{x}_2 + v + L_f z \\ z = A_{12}\hat{x}_2 \end{cases} \tag{19}$$

Auxiliary variable $z = A_{12}\hat{x}_2 = \dot{y} - A_{11}y - B_1 u$ has to be used to estimate rotational speed, which means that the derivative of y has to be measured. To avoid the derivative of y, another auxiliary variable, w, is used:

$$w = \hat{x}_2 - L_f y \tag{20}$$

$$\begin{cases} \dot{w} = \dot{\hat{x}}_2 - L_f \dot{y} = (A_{22} - L_f A_{21})w + B_0 u + Ey \\ B_0 = B_2 - L_f B_1 \\ E = (A_{22} - L_f A_{21})L_f + (A_{21} - L_f A_{11}) \end{cases} \tag{21}$$

Using equations (19)∼(21), the transient speed can be estimated. And the control scheme of the transient speed observer is as shown in Fig.5. y is the output of the original system (i.e. rotational crank angle) and the value of y can be acquired by the crank angle real-time calculation method. T_{eng} can be calculated by average speed and cylinder pressure. T_{ISG} can be replaced by the command torque of the ISG motor. Thereby, transient speed can be estimated from the speed observer, as shown in Fig.6.

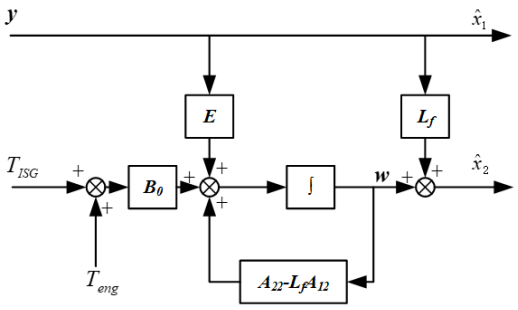

FIGURE 6. Control scheme of transient speed observer.

The error of the transient speed observer established above is shown in Fig.7. The measured speed is shown by the black line and the estimated speed is shown by the red dotted line. The estimated speed is almost the same as the measured speed. And the error is shown in the dotted and dashed

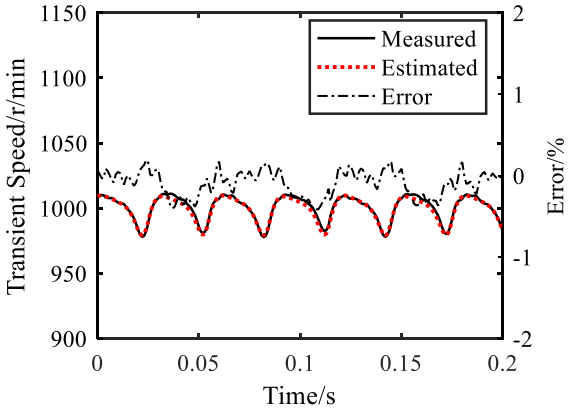

FIGURE 7. Error of transient speed observer at stable state.

line. For the working condition shown in Fig.7, the error is within 1%. Hence, the transient speed observer is capable of calculating the speed fluctuation range accurately.

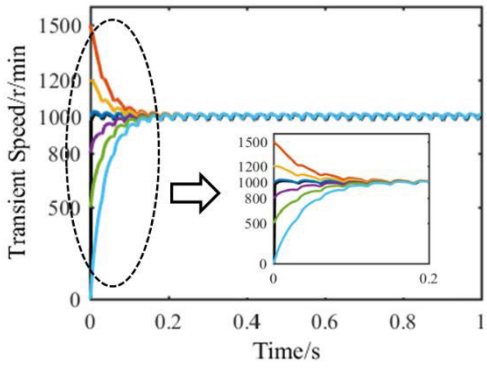

FIGURE 8. Influence of initial speed on transient speed estimation.

When using the transient speed observer to estimate the speed value, initial speed is generally unknown. However, the transient speed observer established above is not dependent on the initial speed value, as shown in Fig.8. Regardless of the initial speed value, the speed curve always converges to the right speed curve within 0.2s. Hence, the transient speed observer is suitable for online application as it is highly accurate, is independent of initial speed, and gives a quick response.

III. DIFFERENT COMPENSATION DESIGN AND ANALYSIS

In the first section, seven kinds of compensation torque waveforms have been designed and they are divided into four groups. The first group of waveforms is waveform 1 and it is designed to represent the traditional vibration control. The first group is used as a control group to compare with the others. The second group of waveforms consists of waveform 2 and waveform 3 and they are designed to represent for the ideal waveform. The design approach of waveform 2 is the most commonly-used method in previous research. The third group of waveforms is designed as digital signals. In this paper, and it contains three kinds of waveforms (waveforms 4, 5, and 6). Waveform 4 is a square wave while waveform 5 and 6 are PWM waveforms. The last group of waveforms (waveform 7) combines the features of waveform 2 and waveform 6 and it is designed as a compromise between the ideal waveform and the square wave.

The second section of this part is the discussion of main causes of vibration and the influence of the deformation of compensation torque converting from an analog signal to a digital signal. Fast Fourier transform (FFT) has been used for analysis. The changes of the ideal waveform and the square waveform are compared in this section as well.

In the last section, experiments are set up to research the relationship between waveforms and the effect of vibration control. The experiment results will be discussed in the next part.

A. DESIGNING THE COMPENSATION TORQUE

The details of the experiment results are discussed in the next few sections. And, in this section, this paper will introduce how to design different waveforms.

In order to answer the question that which kind of compensation design is more suitable for real situation, new kinds of waveforms should be researched and compared. The principle of waveform design is that the waveform should be suitable for online application in an embedded system and it is commonly used. The waveform that satisfies the condition are square waves, triangular waves, trapezoidal waves, sine waves, PWM waves etc. However pre-experiments show that waveform 2∼7 designed have better performance in reducing vibration than other waveforms. To save space, only waveform 2∼7 are discussed in this paper. And waveform 1 is designed representing for the traditional vibration control method and it is used as a control group.

1) WAVEFORM 1

waveform 1 is designed to represent the traditional vibration control with a flywheel. The structure of the range extender used in this paper is somewhat unique, with the rotor of the ISG motor replacing the original flywheel. Hence, waveform 1 is designed to compensate for the difference of inertia. The engine used in this paper has a flywheel whose inertia is 120gm^2 at first. Now replace the flywheel with the ISG motor's rotor. The new inertia is reduced to 84 gm^2. Thus, the ISG motor needs to output extra compensation torque to simulate the difference of inertia. Waveform 1 designed for experiments is shown in Fig.9 (a)

2) WAVEFORM 2

waveform 2 is designed in the shape of the real ripple torque of the engine but with opposite phase. And waveform 2 is the result calculated from equations (5) ∼(13). The cylinder pressure used for calculation is provided by pressure sensors in cylinders. Waveform 2 designed for experiments is shown in Fig.9 (b).

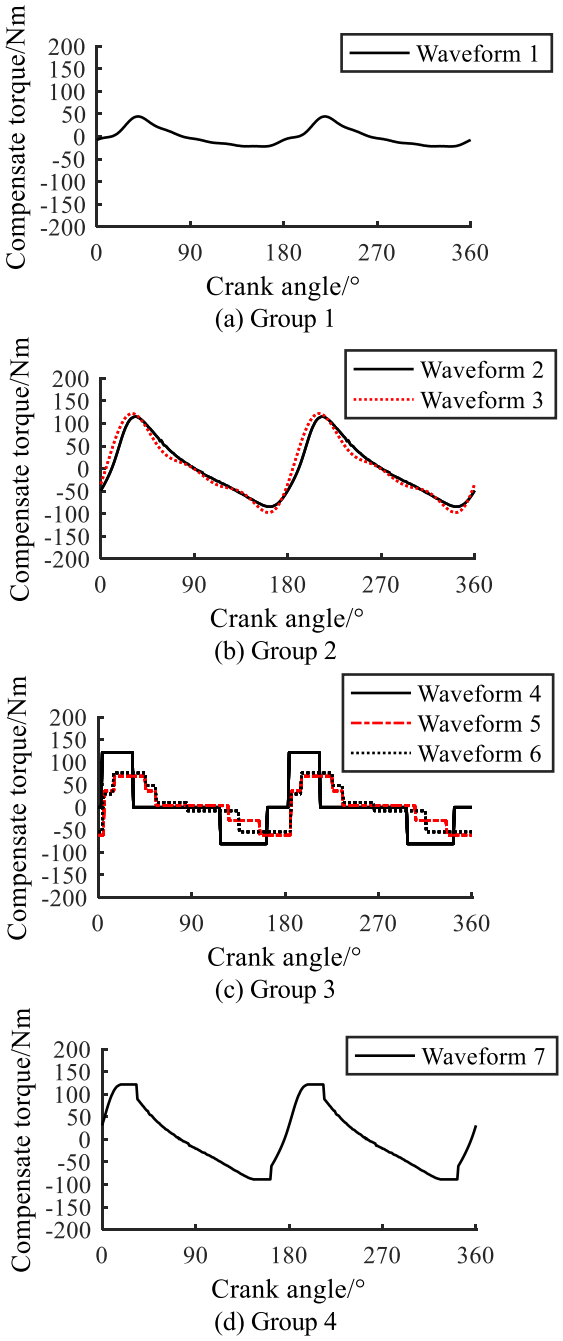

FIGURE 9. Designing of different waveforms.

3) WAVEFORM 3

waveform 3 is also designed in the shape of the real ripple torque of the engine but with opposite phase. However, waveform 3 is the adding-up of the first three order harmonics of the engine torque Fourier transform results instead of the results calculated from equations (5)∼(13). Waveform 3 designed for experiments is shown in Fig.9 (b).

4) WAVEFORM 4

waveform 4 is the square waveform proposed in this paper. Waveform 4 designed for experiments is shown in Fig.9 (c). The black line is waveform 4 and the red line is the trajectory of waveform 2. Waveform 4 and waveform 2 have equal positive semi-axial areas and equal negative semi-axial areas

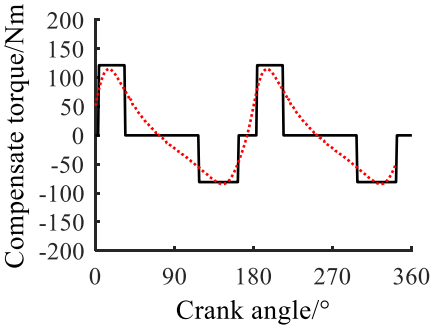

FIGURE 10. Designing process of waveform 4.

5) WAVEFORMS 5&6

waveform 5 and waveform 6 are square waveforms as well and they are designed according to pulse width modulation (PWM).

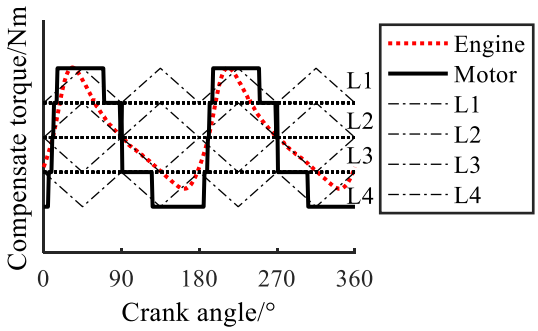

FIGURE 11. Pulse width modulation.

Fig.11 shows the process of pulse width modulation (waveform 5). L1∼L4 are the reference triangle wave. And the curve of the engine ripple torque is shown by a red line. If the torque of the engine is bigger than L2, then the compensation torque of the motor will be set to the maximum value of L2. And if the torque of the engine is bigger than L1, then the compensation torque of the motor will be set to the maximum value of L1. If the torque of the engine is smaller than L3, then the compensation torque of the motor will be set to the minimum value of L3. And if the torque of the engine is smaller than L4, then the compensation torque of the motor will be set to the minimum value of L4. The design process is the same as for waveform 6 except that six triangle waves are used in the design. If the design process is compared with the sine pulse width modulation process of the electric motor, the design of waveform 5 is the process of '2-level SPWM' and the design of waveform 6 is the process of '3-level SPWM'.

6) WAVEFORM 7

waveform 7 is the combination of waveform 2 and waveform 4 and it is used as a compromise between the most

commonly-used method and the novel way. The red line in Fig.12 is waveform 2 and the blue line in Fig.12 is waveform 4. Square waves are used near the extremums.

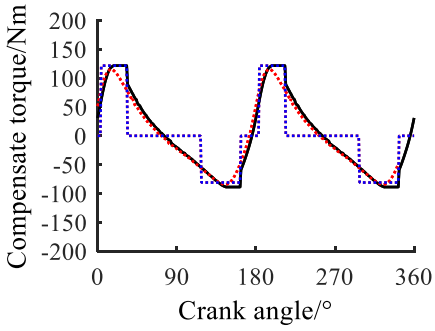

FIGURE 12. Designing process of waveform 7.

B. DEFORMATION OF WAVEFORM

This section is focusing on explaining for the reasons why the ideal waveform is not the optimal waveform considering real situation. The reasons are: (1) the deformation of the ideal waveform considering control cycle and time delay makes it not suitable for active damping control; (2) The suspension system of a range extender may change the vibration characteristics. Simulations are conducted to illustrate these situation.

1) REASON (1)

the deformation of the ideal waveform is shown in Fig.13. The ideal waveform is similar to the torque of engine but with opposite phase. If the control cycle of MUC is taken into consideration, the ideal waveform will turn into the command torque as shown in Fig.13 (red line). If the time delay is taken into consideration, the actual output torque of ISG motor is shown by the black line in Fig.13. The actual output torque has been seriously deformed compared with the ideal torque. Hence, it may not be the optimal waveform anymore.

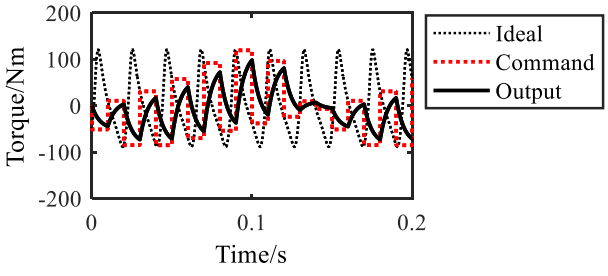

FIGURE 13. Deformation of the ideal waveform.

The comparison of the Ideal waveform (Waveform 2) and the square waveform (Waveform 4) is shown in Fig.14. Considering real situation, the square waveform may perform better than the ideal waveform. The reason is: in the case of similar shapes, the square waveform has bigger amplitude compared with the ideal waveform, which means that the torque fluctuation of the total torque (engine torque adding-up with the ISG motor torque) is smaller when the compensation torque is designed as the waveform 4. Hence, the excitation of vibration may be smaller when using waveform 4 as the compensation torque.

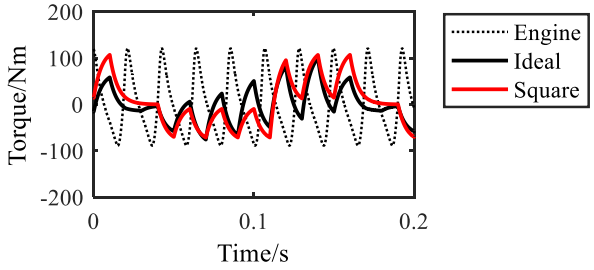

FIGURE 14. Comparison between the ideal waveform and the square waveform.

2) REASON (2)

The suspension system of a range extender may change the vibration characteristics. Hence,the main causes of vibration should be figured out. Hence, Fourier transform is used to analyze the frequency spectrum of vibration in different directions. Results are shown in Fig.15.

The engine is controlled with 1400r/min speed in Fig.15. Thus, the basic frequency is about 46.7Hz. And 93.3Hz is the frequency of the 2^{nd}-order harmonic. Generally, the first three order harmonics are the main causes of vibration. But there are some differences in each direction. According to the results, the main reason for axial vibration and motor vibration is the first two order harmonics. The main cause of top vibration is the first three order harmonics of engine torque. As for the block vibration, not only are the first two order harmonics the main cause, some high-order harmonics also make a contribution. Thereby, not just the first three order harmonics should be considered when using active damping control, some higher-order harmonics (270Hz∼360Hz) should also be reduced in the meantime. However, the frequency spectrum of the ideal waveform (waveform 2) has smaller amplitude in the high frequency band than the square waveform as shown in Fig 16. Hence the ideal waveform may perform worse than the square waveform in reducing block vibration.

To sum up, the ideal waveform may not be the optimal waveform considering the real situations.

C. EXERIMENT SETUP

To verify assumptions made in section B, a test bench is set up for testing the vibration performance and effect of active damping control. The overall test bench is shown in Fig.13. There are three parts of the whole test bench: (1) range extender; (2) controlling system; (3) sensors and mounting.

The range extender is shown in Fig.17. It has an inline four-cylinder gasoline engine and an ISG motor replacing the original flywheel of the engine. The ISG motor is powered by

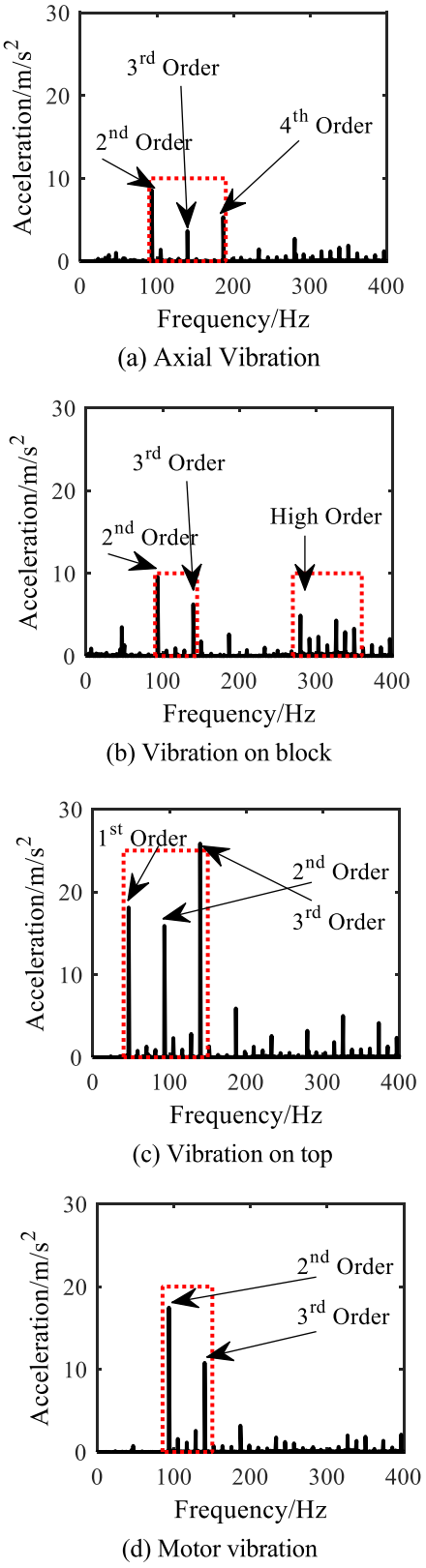

FIGURE 15. Main causes of vibration.

a battery simulator. When working in a steady state, the ISG motor is used as the load of the engine and it will charge the battery. When working in the start-up process, the ISG motor

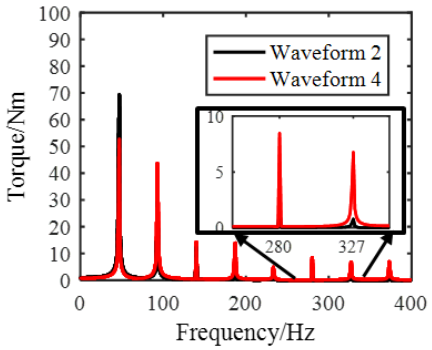

FIGURE 16. FFT of waveform 2 and waveform 4.

is used as a starter to drag the whole system up and the battery will discharge. Parameters of the range extender are listed in Table 1.

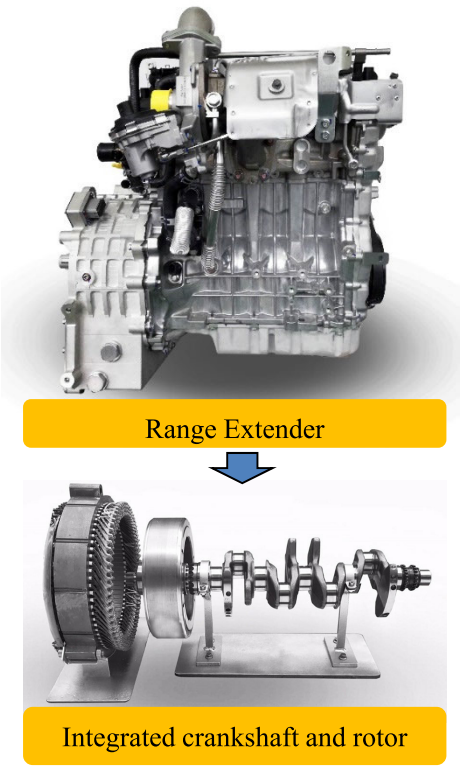

FIGURE 17. Range extender and its crankshaft.

The whole controlling system consists of the MCU, ECU, and upper computer. The upper computer has the same function as the vehicle control unit (VCU) in a real hybrid vehicle. It will give the speed target and torque target to the MCU and ECU through controller area network (CAN) communication.

The range extender is mounted to the ground with three legs (Fig.18). Leg 1 is fixed to the cylinder block of the engine. Leg 2 and Leg 3 are fixed to the end surface of the shell of the ISG motor. In addition, at the junction with the legs there are rubber gaskets. Leg 1, Leg 2, Leg 3 and the rubber gaskets form the whole suspension system.

The placement of the sensors is shown in Fig.19. There are two different kinds of indexes to research the performance of

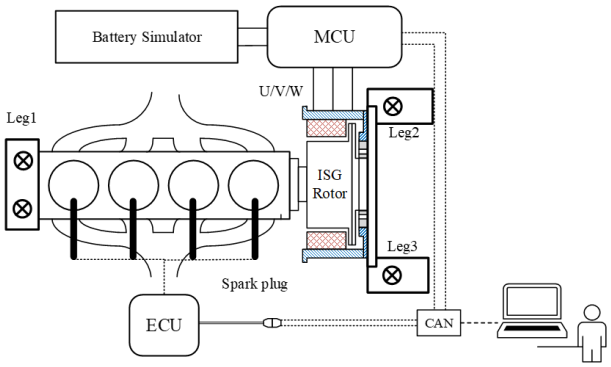

FIGURE 18. Overall test bench.

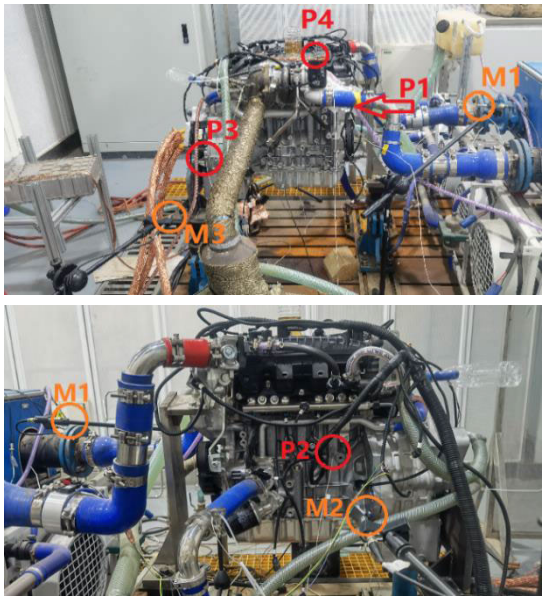

FIGURE 19. Placement of acceleration sensors and microphones.

TABLE 1. Parameters of the range extender.

Components	Parameters	Value
Engine	Displacement	1.48L
	Air Intake	Turbo
	Compress Ratio	11.5
	Max. Net Power	120kW@5600rpm
	Max. Net Torque	230Nm@2000~4500rpm
	Max. Speed	6300rpm
	Ignition Sequence	1-3-4-2
ISG Motor	Rated Power	70kW
	Rated Voltage	350V
	Rated Speed	2800rpm
	Rated Torque	230Nm
	Max. Power	90kW
	Max. Speed	6000rpm
	Max. Torque	280Nm
	Max. Efficiency	97%

active damping control under different compensation torque waveforms. They are: (1) vibration acceleration in different directions; and (2) speed fluctuation. Vibration acceleration is acquired by acceleration sensors (P1∼P4). P1 is mounted on the housing of the output shaft, which is called axial vibration in the next few sections. P2 is mounted on the housing of the block near the intake manifold, which is called block vibration in the next few sections. P3 is mounted on the surface of the motor's shell, which is called motor vibration in the next few sections. And P4 is mounted on the top of the cylinder head, which is called top vibration in the next few sections. Speed fluctuation is acquired from the data of the motor's resolver. It is important to mention that sound pressure is also tested by microphones (M1∼M3). However, there is no obvious change in sound pressure whether using active damping control or not. Thus, there is no discussion about sound performance in this paper.

The speed of the range extender is controlled to be 1400r/min and the load is set to 20%. The speed is controlled to 1400r/min because it is the point where speed fluctuation reaches the biggest. As for the reason why the load is set up to 20%, it is considering the maximum torque of the ISG motor. If the load is set up too high, the average torque will be close to the limitation and the amplitude of the compensation torque will too small to verify the influence of different kinds of waveforms. Hence, 20% is set up to be the load in the experiments.

IV. EXPERIMENT RESULTS AND DISCUSSION

A. EFFECTIVENESS OF ACTIVE DAMPING CONTROL

In this section, experiments are conducted to prove the effectiveness of active damping control. The transient acceleration in the time domain consists of harmonics with all frequencies. It is difficult to show the effectiveness of active damping control clearly using transient acceleration in the time domain. Hence, the root mean square (RMS) value of acceleration is chosen to evaluate the vibration and short-time Fourier transform (STFT) is used in the analysis process. STFT can not only show information about the frequency spectrum but can also show information in the time domain. The results of active damping control with compensation torque in the shape of waveform 4 are as shown in Fig.20.

As shown in Fig.20, active damping control is disabled during the first second and it is enabled after 1s. The brighter the line is, the bigger the amplitude of the harmonic is. Generally, the color is dimmer when active damping control is enabled, which means that active damping control can reduce vibration in different directions effectively.

When active damping control is disabled, axial vibration is mainly excited by harmonics with frequency of 93Hz, 140Hz, and 188Hz (2^{nd} order, 3^{rd} order, and 4^{th} order). After using active damping control, the amplitude of 2^{nd}- and 4^{th}-order harmonics is reduced. And block vibration is mainly excited by 2^{nd}-order harmonic and some high-order harmonics. After using active damping control, the color of the 2^{nd} order and some higher order (the frequency is about 300Hz or 350Hz) is dimmer. However, the amplitude is larger for the 4^{th}-order and some high-order (above 350Hz) harmonics, which means using square waves creates additional vibrations in the higher

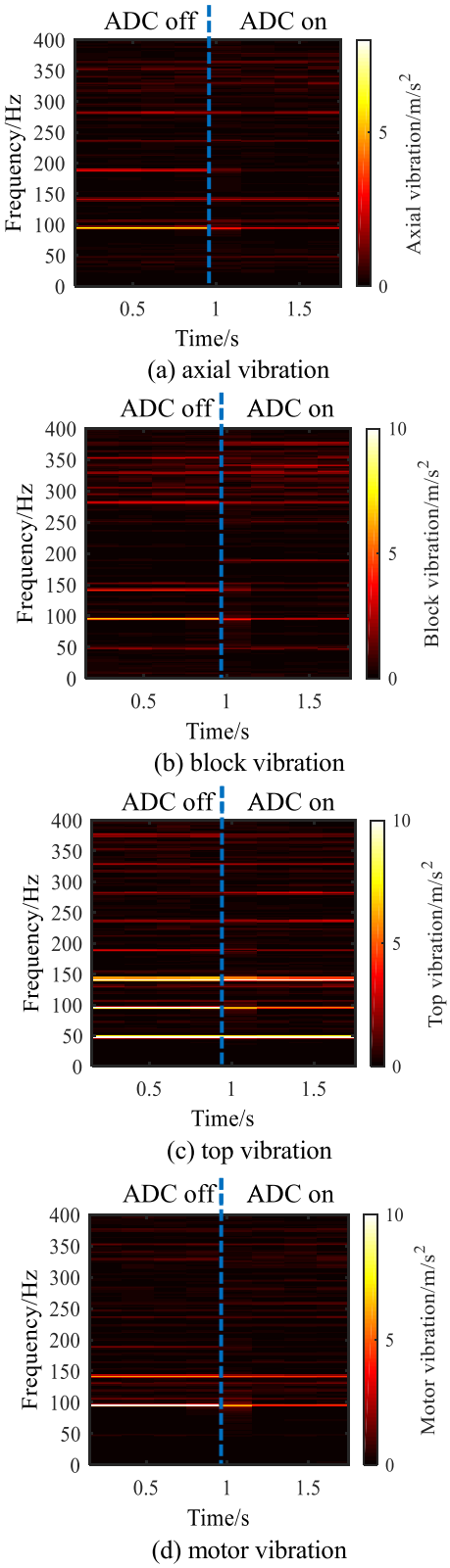

FIGURE 20. STFT of vibration acceleration in different directions.

frequency bands. As for top vibration, the brightest lines are the first three order harmonics. Although the color is dimmer after using active damping control, there are still some bright lines, which means top vibration is still worth paying attention to. The main causes of motor vibration are the 2nd-order and 3rd-order harmonics. After using active damping control, they are both reduced.

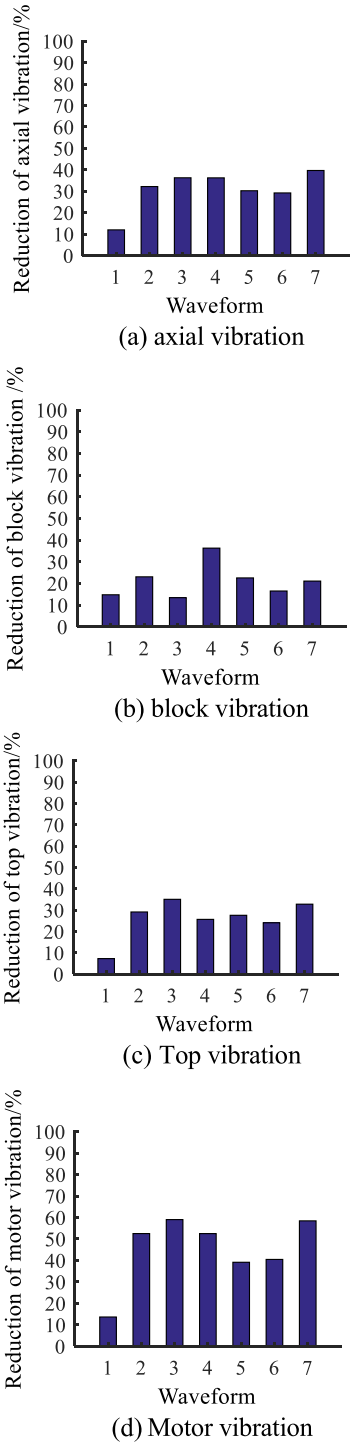

FIGURE 21. Reduction of vibration using different kinds of waveforms on acceleration in different directions.

B. COMPARSION OF DIFFERENT WAVEFORMS

The effectiveness has been proven in the last section. In this section, the effects of different waveforms on vibration

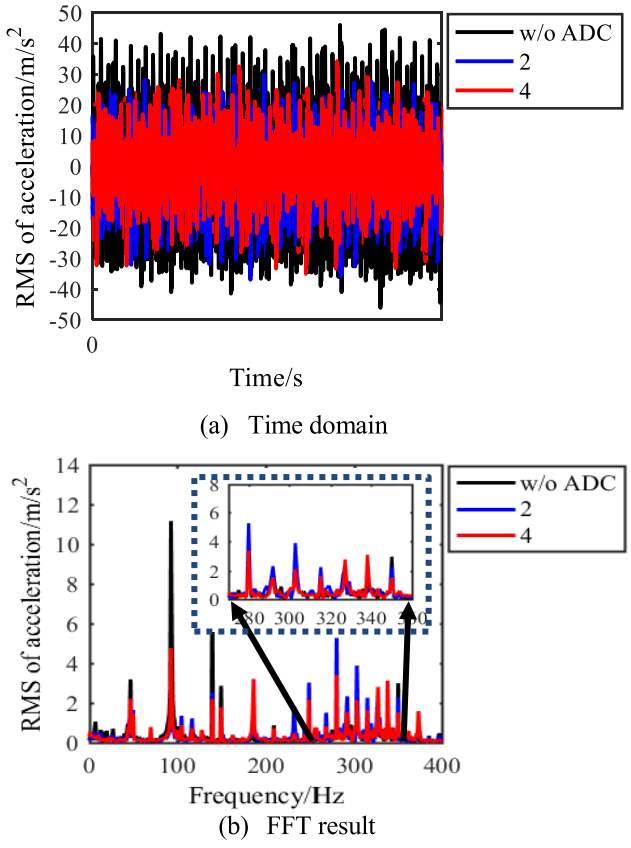

FIGURE 22. Comparison of waveform 2 and waveform 4.

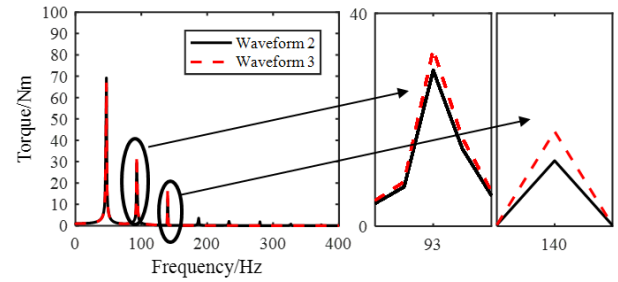

FIGURE 23. FFT of waveform 2 and waveform 3.

reduction are compared and assumptions made in section B of the previous part are proven in this part.

Statements can be drawn from Fig 21.

1) STATEMENT 1

reduction of vibration when using traditional vibration control is generally within 15%. However, when using active damping control, the reduction of vibration is usually bigger than 24% except for block vibration. Hence, active damping control is recommended for controlling vibration in the range extender.

2) STATEMENT 2

waveform 7 is designed as a compromise between the most commonly-used method and the novel way. It has a better performance in reducing axial vibration, top vibration, and motor

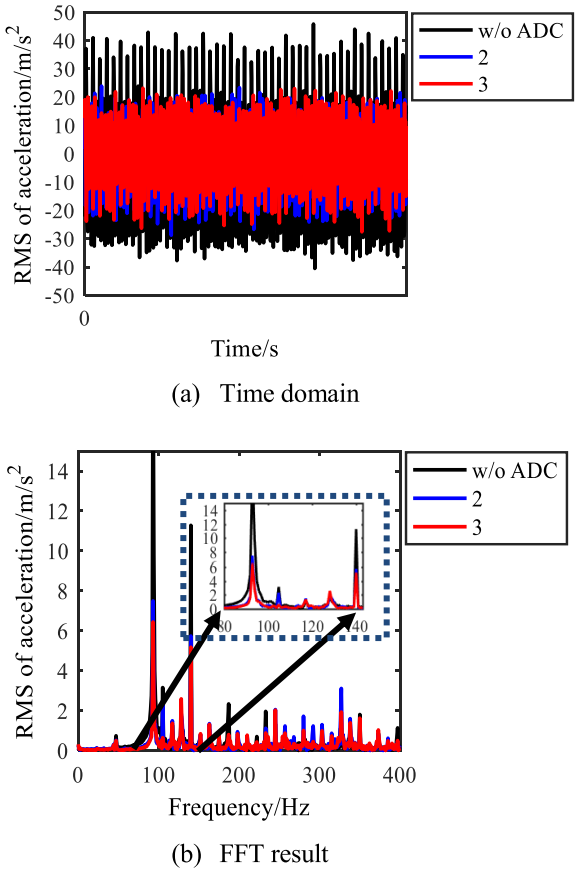

FIGURE 24. Comparison of waveform 2 and waveform 3.

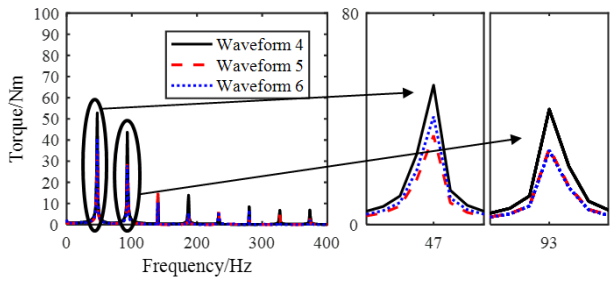

FIGURE 25. FFT of waveform 4, waveform 5 and waveform 6.

vibration. On some occasions, it may perform better than waveform 2 and waveform 4. However, the performance of waveform 7 in reducing cylinder vibration is not satisfactory.

3) STATEMENT 3

active damping control with compensation torque in the shape of waveform 4 has potential in reducing vibration in all directions. The reason have been discussed in the previous part (section B).The reduction of block vibration can reach 36.3% whilst the others are less than 25%.The reason why waveform 4 can reduce block vibration is that the square wave usually has bigger amplitude of higher-order frequency harmonics while the main excitation of block vibration is the 2nd-order and some high-order harmonics. Hence, waveform 4 is more suitable in active vibration control.

	A_{pp}	A_{rms}	A_{max}	A_{min}	S_P	S_N	A_{f1}	A_{f2}	A_{f3}	A_{f4}
Min. axial vibration	-0.84	-0.88	-0.82	0.85	-0.74	-0.65	-0.71	-0.97	-0.85	-0.40
Min. block vibration	-0.10	-0.15	-0.13	0.06	0.14	-0.10	0.11	-0.52	-0.14	-0.93
Min. top vibration	-0.84	-0.84	-0.76	0.91	-0.88	-0.87	-0.80	-0.72	-0.93	0.16
Min. motor vibration	-0.94	-0.96	-0.91	0.96	-0.89	-0.71	-0.87	-0.91	-0.89	-0.14
Axial Vibration reduction	0.91	0.94	0.87	-0.93	0.87	0.73	0.83	0.90	0.88	0.18
block vibration reduction	0.36	0.39	0.41	-0.29	0.09	0.12	0.16	0.66	0.27	0.90
Top Vibration reduction	0.87	0.88	0.81	-0.94	0.90	0.85	0.83	0.77	0.92	-0.09
Motor Vibration reduction	0.97	0.98	0.94	-0.98	0.94	0.69	0.92	0.86	0.86	0.05

FIGURE 26. Correlation between designing factors and vibration indicators.

Fig.22 shows the results of Fourier transform of the block vibration. The black line is the RMS of block vibration when active damping control is disabled. The blue line is the RMS of block vibration when active damping control is enabled while the compensation torque is in the shape of waveform 2. The red line is the RMS of block vibration when active damping control is enabled while the compensation torque is in the shape of waveform 4. In the frequency range of 270Hz to 360Hz, the amplitude of the red line is smaller than that of the blue line, which means that waveform 4 can reduce vibration in high frequency bands.

4) STATEMENT 4

waveform 2 and waveform 3 both represent the ideal waveform except that waveform 2 is the calculation result of equation (5)∼equation (13) while waveform 4 only has the first three order harmonics of the calculation result. The result (Fig.23) shows that waveform 3 has bigger amplitude of 2nd- and 3rd-order harmonics than waveform 2. Hence, it may perform better in reducing axial vibration, top vibration, and motor vibration (especially motor vibration that is mainly excited by 2nd- and 3rd-order harmonics).

Results shown in Fig.21 prove this statement. The reduction of axial vibration, top vibration, and motor vibration are 32.2%, 29.2%, and 52.5% respectively when the compensation torque is in the shape of waveform 2. And the reduction of axial vibration, top vibration, and motor vibration is 36.3%, 35.1%, and 59.3% respectively when the compensation torque is in the shape of waveform 2.

Fig.24 shows the results of Fourier transform of the motor vibration. The black line is the RMS of motor vibration when active damping control is disabled. The blue line is the RMS of motor vibration when active damping control is enabled while the compensation torque is in the shape of waveform 2. The red line is the RMS of motor vibration when active damping control is enabled while the compensation torque is in the shape of waveform 3. The amplitude of 2nd-order and 3rd-order harmonics with compensation in the shape of waveform 3 is smaller than the amplitude of 2nd-order and 3rd-order harmonics with compensation in the shape of waveform 2. And this result is also proved with the analysis above.

5) STATEMENT 5

waveform 4, waveform 5, and waveform 6 all represent the square wave except that waveform 5 and waveform 6 are designed using PWM. The reduction of vibration with compensation torque in the shape of waveforms 4, 5, and 6 is summarized in Table 2.

TABLE 2. Comparison of waveform 4, 5, and 6.

Waveform	Reduction			
	Axial vibration	Block vibration	Top vibration	Motor vibration
4	36.3%	36.3%	25.7%	52.5%
5	30.2%	22.5%	27.6%	39.2%
6	29.2%	16.5%	24.1%	40.5%

The results can also be explained by FFT as shown it Fig 25. Waveform 4, waveform 5 and waveform 6 are all represent for the square wave except that waveform 5 waveform 6 are designed using PWM. The result is that the amplitude of waveforms modulated with PWM are generally smaller than that of simply square wave (waveform 4). It is easy to expect that the performance of waveform 5 waveform 6 will not be as effective as waveform 4.

V. CORRELATION BETWEEN DESIGN FACTORS AND VIBRATION REDUCTION

Amplitude of harmonics of different orders is an important design factor for compensation torque. However, it is not the only design factor. There are still some other design factors (like the average amplitude, the maximum value of amplitude, etc.) that will have an influence on vibration improvement. In this section, the relationship between design factors and vibration reduction is revealed through correlation

analysis. And the result can be used to guide the compensation torque design process.

The mathematical way adopted by this paper is correlation. Correlation between two sequences can explain their relationship.

$$R = \frac{Cov(X, Y)}{\sqrt{Var(X) \cdot Var(Y)}} \tag{22}$$

$$Cov(X, Y) = \sum \left(X - \bar{X}\right)(Y - \bar{Y}) \tag{23}$$

$$Var(X) = \sum \left(X - \bar{X}\right)^2 \tag{24}$$

$$Var(Y) = \sum \left(Y - \bar{Y}\right)^2 \tag{25}$$

where X is one sequence, Y is the other sequence. $\bar{X}$ is the average value of X, and $\bar{Y}$ is the average value of Y. in this paper, X can be any design factor and Y can be any vibration indicator. Correlation R is limited to range [−1,1]. When the absolute value of R is closer to 1, then X and Y are more related.

Design factors used in this paper are:

(1) **Amplitude:** peak-peak amplitude A_{pp}, root-mean-square value of amplitude A_{rms}, maximum value of amplitude A_{max}, and minimum value of amplitude A_{min}.

(2)**Area:**the area of positive part S_P and the area of negative part S_N.

(3) **FFT results:** the amplitude of the first 4th-order harmonics (A_{f1},A_{f2}, A_{f3} and A_{f4}) of discrete-time Fourier transform (DFT) of compensate torque value.

Vibration indicators used in this paper are:

(1) Minimum value of acceleration in different directions including minimum axial vibration, minimum block vibration, minimum top vibration, and minimum motor vibration.

(2) Reduction of the acceleration value by using active damping control including axial vibration reduction, block vibration reduction, top vibration reduction, and motor vibration reduction.

(3) Reduction of speed fluctuation.

The correlation between geometric parameters and vibration indicators is shown in Fig.26; green means the correlation is positive and blue means the correlation is negative. The darker the color, the stronger the correlation. This figure can be used as a guiding tool for adjusting compensation torque design without detecting the vibration acceleration. The steps are as follow:

Step 1: requirements of reducing vibration need to be required.

Step 2: The correlation coefficient is get from the guiding tool according to the main requirement.

Step 3: The main design factors can be chosen by the correlation coefficient. If the correlation coefficient is big enough, the design factors corresponding to the correlation coefficient is chosen as the main design factor. It is recommended to select design factors with a correlation coefficient greater than 0.9. For example, the main requirement is to reduce the vibration of cylinder block, then the main design factor is chosen to be the amplitude of the t 4th-order harmonics, A_{f4}.

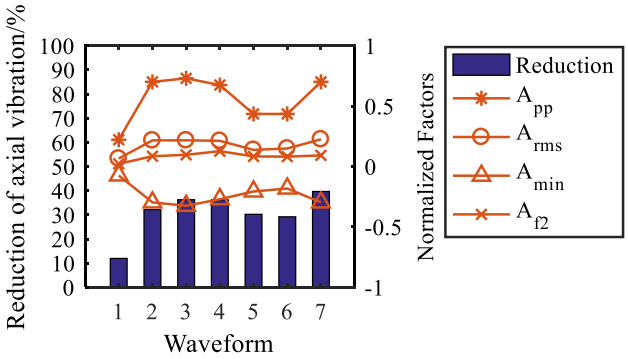

(a) axial vibration reduction and normalized design factors

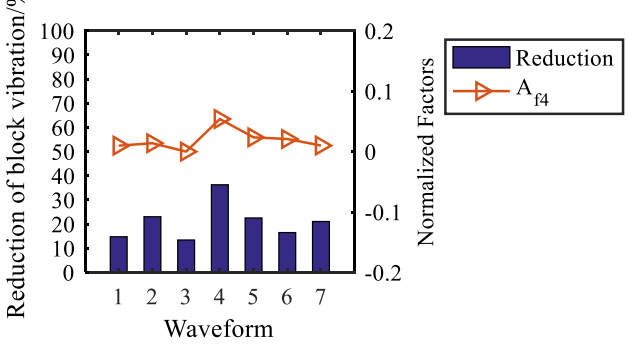

(b) right vibration reduction and normalized design factors

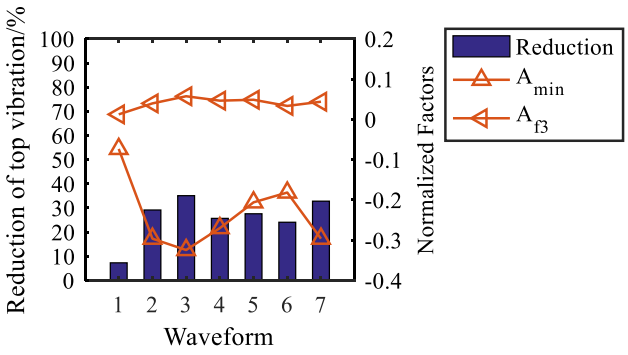

(c) top vibration reduction and normalized design factors

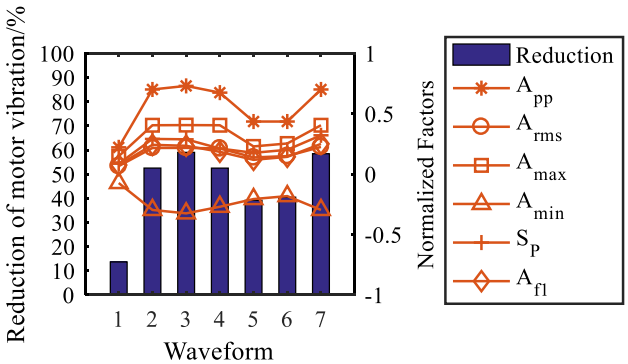

(d) motor vibration reduction and normalized design factors

FIGURE 27. The relationship between normalized main design factors and vibration reduction.

Step 4: Normalize the main design factors. Main design factors except for S_P and S_N should be divided by the

maximum torque of the motor (T_{max}). And S_P, S_N should be divided by πT_{max}.

Step 5: If the correlation coefficient is positive, the main factors need to be designed with bigger value. If the correlation coefficient is negative, the main factors need to be designed with smaller value.

Taking our compensation torque design as an example, the main design factors to reduce axial vibration are: A_{pp},A_{rms}, A_{min} and A_{f2}. The main design factor to reduce block vibration is A_{f4}. The main design factors to reduce top vibration are:A_{min} and A_{f3}. The main design factors to reduce motor vibration are: A_{pp},A_{rms}, A_{max}, $A_{min}S_P$ and A_{f1}(are not selected to avoid duplication). The relationship between main design factors and vibration reduction is shown in Fig.27.

As shown in Fig.27, if the correlation coefficient is positive, the bigger the value of normalized design factors is, the more the reduction. If the correlation coefficient is negative, the bigger the value of normalized design factors is, the less the reduction. Depending on the main design factors and vibration damping requirements, the corresponding waveform can be adjusted. For example, if the vibration damping requirement is to reduce the block vibration and the waveform designed in the shape of waveform 5 (a PWM wave shown in Fig.9), then the amplitude of the 4th order harmonic should be enlarged by designing to satisfy your vibration damping requirement.

VI. CONCLUSION

The conclusion are summarized as follows:

1) An active damping control method based on transient speed observer has been established at first. Experiment results show that active damping control can suppress vibration effectively. The vibration acceleration can be reduced by 39.7% to 59.0% (with appropriate compensation torque) while the reduction of traditional vibration control is generally within 15%.
2) A transient speed observer has been established in this paper. The error of the speed observer is within 1% and the time delay is within 0.2s. Hence, it is suitable for online application as it is highly accurate, is independent of initial speed, and gives a quick response.
3) The question what kind of compensation torque design is more suitable for online application has been answer through experiments and FFT analysis. The ideal waveform is more suitable for reducing top vibration and motor vibration while the square waveform is more suitable for reducing block vibration. And the waveform combining the feather of these two waveforms is more suitable for reducing axial vibration. And the square waveform is recommended for the optimal waveform based on our experiment results because of its potential to reduce vibration effectively in all directions.
4) A guiding tool for adjusting compensation torque design without detecting the vibration acceleration is summarized using correlation analysis. And it can be used for guiding compensation torque design by calculating design factors.

Suggestions for future work are as follows:

1) Some advanced control methods can be applied to the active damping control [32].
2) Although the square wave is recommended for active damping control, some problems still exist. Using the square wave may cause some extra vibration in the high frequency band. And further research concerning the optimal waveform is still needed.
3) The relationship between design parameters and vibration indicators is qualitative. Perhaps quantitative relationship can be established through mathematical methods.

REFERENCES

[1] Y. Yang, Y. Zhang, J. Tian, and T. Li, "Adaptive real-time optimal energy management strategy for extender range electric vehicle," *Energy*, vol. 197, Apr. 2020, Art. no. 117237, doi: 10.1016/j.energy.2020.117237.

[2] D.-M. Kim, P. Benoliel, D.-K. Kim, T. H. Lee, J. W. Park, and J.-P. Hong, "Framework development of series hybrid powertrain design for heavy-duty vehicle considering driving conditions," *IEEE Trans. Veh. Technol.*, vol. 68, no. 7, pp. 6468–6480, Jul. 2019, doi: 10.1109/TVT.2019.2914868.

[3] A. Rust and B. J. Graf, "NVH of electric vehicles with range extender," *SAE Int. J. Passenger Cars Mech. Syst.*, vol. 3, no. 1, pp. 860–867, Jun. 2010, doi: 10.4271/2010-01-1404.

[4] R. Guo, C. Cao, Y. Mi, and Y. Huang, "Experimental investigation of the noise, vibration and harshness performances of a range-extended electric vehicle," *Proc. Inst. Mech. Eng., D, J. Automobile Eng.*, vol. 230, no. 5, pp. 650–663, Apr. 2016, doi: 10.1177/0954407015591329.

[5] L. Zhang, W. Chen, D. Meng, G. U. Peng, and Z. Yu, "Vibration analysis of series-parallel hybrid powertrain system under typical working condition and modes," Tongji Univ., Shanghai, China, SAE Tech. Paper 2018-01-1291, 2018, doi: 10.4271/2018-01-1291.

[6] J. Zhang and W. Gao, "Influence of first order reciprocating inertia moment balance ratio on torsional vibration and surface vibration of crankshaft for three-cylinder engine," *Mech. Sci. Technol. Aerosp. Eng.*, vol. 39, no. 10, pp. 1477–1482, 2020, doi: 10.13433/j.cnki.1003-8728.20190304.

[7] Z. Longbao, *Internal Combustion Engines*. China: China Machine Press, 2011.

[8] P. Hooper, "Novel three-cylinder engine solutions offering low noise vibration and harshness for range-extender and hybrid electric vehicles," Auckland Univ. Technol., Auckland, New Zealand, SAE Tech. Paper 2018-01-1553, Jan. 2018, doi: 10.4271/2018-01-1553.

[9] S. V. Gusev, W. Johnson, and J. Miller, "Active flywheel control based on the method of moment restrictions," in *Proc. Amer. Control Conf.*, 1997, pp. 3426–3430.

[10] A. T. Zaremba, I. V. Burkov, and R. M. Stuntz, "Active damping of engine speed oscillations based on learning control," in *Proc. Amer. Control Conf. (ACC)*, 1998, pp. 2143–2147.

[11] A. T. Zaremba and R. I. Davis, "Control design for active engine damping using a starter/alternator," in *Proc. Amer. Control Conf. (ACC)*, vol. 3, Jun. 2000, pp. 2043–2047.

[12] M. Beuschel, M. Rau, and D. Schroder, "Adaptive damping of torque pulsation using a starter generator-opportunities and boundaries," in *Proc. Conf. Rec. IEEE Ind. Appl. Conf. 35th IAS Annu. Meeting World Conf. Ind. Appl. Electr. Energy*, vol. 5, 2000, pp. 1403–1408.

[13] K. Nakano and S. Ochiai, "Development of the motor-assist system for the hybrid automobile–the insight development of the motor-assist system for a hybrid car–insight," Honda R&D, Saitama, Japan, SAE Tech. Paper 2000-01-C079, 2000.

[14] B. Badreddine, A. Zaremba, J. Sun, and F. Lin, "Active damping of engine idle speed oscillation by applying adaptive PID control," Ford Motor Company, Wayne State Univ., Detroit, MI, USA, Tech. Rep. 2001-01-0261.
[15] S. Tomura, Y. Ito, K. Kamichi, and A. Yamanaka, "Development of vibration reduction motor control for series-parallel hybrid system," Toyota Central R&D Labs, Toyota Motor Corp., Yokomichi, Japan, SAE Tech. Paper 2006-01-1125, 2006, doi: 10.4271/2006-01-1125.
[16] Y. Ito, S. Tomura, and S. Sasaki, "Development of vibration reduction motor control for hybrid vehicles," in *Proc. IECON 33rd Annu. Conf. IEEE Ind. Electron. Soc.*, Taipei, Taiwan, Nov. 2007, pp. 516–521, doi: 10.1109/IECON.2007.4460237.
[17] F. U. Syed, M. L. Kuang, and H. Ying, "Active damping wheel-torque control system to reduce driveline oscillations in a power-split hybrid electric vehicle," *IEEE Trans. Veh. Technol.*, vol. 58, no. 9, pp. 4769–4785, Nov. 2009, doi: 10.1109/TVT.2009.2025953.
[18] Y. Kou and F. Weslati, "Development of a hybrid powertrain active damping control system via sliding mode control scheme," Chrysler Group LLC, Auburn Hills, MI, USA, SAE Tech. Paper 2013-01-0486, 2013, doi: 10.4271/2013-01-0486.
[19] R. Guo and X. Liu, "Active launch vibration control of power-split hybrid electric vehicle considering nonlinear backlash," *SAE Int. J. Adv. Curr. Prac. Mobility*, vol. 3, no. 4, pp. 2087–2097, 2021, doi: 10.4271/2021-01-0667.
[20] R. I. Davis and R. D. Lorenz, "Engine torque ripple cancellation with an integrated starter alternator in a hybrid electric vehicle: Implementation and control," in *Proc. Conf. Rec. IEEE Ind. Appl. Conf. 37th IAS Annu. Meeting*, Pittsburgh, PA, USA, Nov. 2002, pp. 2016–2021.
[21] R. D. Lorenz and R. I. Davis, "Apparatus and method for engine crankshaft torque ripple control in a hybrid electric vehicle," U.S. Patent 6 336 070, Jan. 1, 2002.
[22] R. Guo and M.-J. Wang, "Active control of hybrid electric vehicle launch vibration in pure electric mode," *J. Vibrat. Control*, vol. 24, no. 4, pp. 673–681, Feb. 2018, doi: 10.1177/1077546316648811.
[23] R. Guo, M.-J. Wang, and C. Cao, "Gas torque compensation control for range extender start-stop vibration reduction in electric vehicle," *Proc. Inst. Mech. Eng., I, J. Syst. Control Eng.*, vol. 231, no. 7, pp. 567–581, Aug. 2017, doi: 10.1177/0959651817710146.
[24] R. Guo, S. Han, M.-J. Wang, and C. Cao, "Electric motor-based crankshaft stop position control to suppress range extender start vibration in electric vehicle," *J. Low Freq. Noise, Vibrat. Act. Control*, vol. 37, no. 3, pp. 422–442, Sep. 2018, doi: 10.1177/0263092317711598.
[25] X. Chen, D. Peng, J. Hu, C. Li, S. Zheng, and W. Zhang, "Adaptive torsional vibration active control for hybrid electric powertrains during start-up based on model prediction," *Proc. Inst. Mech. Eng., D, J. Automobile Eng.*, vol. 236, nos. 10–11, pp. 2219–2229, Sep. 2022, doi: 10.1177/09544070211056176.
[26] D. Jiang, Y. Huang, and D. Hao, "Vehicle active damping control with considering time delay," *J. Beijing Inst. Technol.*, vol. 26, no. 4, pp. 449–457, 2017, doi: 10.15918/j.jbit1004-0579.201726.0404.
[27] D. Meng, H. Liu, L. Zhang, and J. Xu, "Analysis and active control of torsional vibration in range extender with internal combustion engine," *J. Vibrat. Control*, pp. 1–16, Apr. 2022, Art. no. 107754632210751, doi: 10.1177/10775463221075119.
[28] L. Du, L. Xu, Y. Hu, M. Ouyang, and F. Yang, "Optimal speed profile for minimum vibration during engine start using Pontryagin's minimum principle approach," Tsinghua Univ., Beijing, China, SAE Tech. Paper 2019-01-5026, 2019, doi: 10.4271/2019-01-5026.
[29] L. Du, F. Yang, Y. Hu, and L. Xu, "Active damping control of torsional vibration in a diesel hybrid powertrain," Tsinghua Univ., Beijing, China, SAE Tech. Paper 2019-01-2342, 2019, doi: 10.4271/2019-01-2342.
[30] Y. Hu, F. Yang, L. Du, J. Zhang, and M. Ouyang, "A novel method to actively damp the vibration of the hybrid powertrain by utilizing a flywheel integrated-starter-generator," *IEEE Access*, vol. 8, pp. 147045–147058, 2020.
[31] Y. Hu, "Study of the high frequency active torque compensation control of the hybrid powertrain," Ph.D. dissertation, School Vehicle Mobility, Tsinghua Univ., Beijing, China, 2021.
[32] Y. Sun, J. Xu, G. Lin, W. Ji, and L. Wang, "RBF neural network-based supervisor control for maglev vehicles on an elastic track with network time delay," *IEEE Trans. Ind. Informat.*, vol. 18, no. 1, pp. 509–519, Jan. 2022.

ZHANG JINYU was born in Chengde, Hebei, China, in 1993. He received the B.S. degree in automotive engineering from Tsinghua University, Beijing, China, in 2016, where he is currently pursuing the Ph.D. degree with the Department of Automotive Engineering. He is the author of two articles. His research interest includes hybrid system control, especially motor control.

HU SONG received the Ph.D. degree from Harbin Engineering University, in July 2019. He spent one year as a Visiting Ph.D. Student with the Department of Energy, Politecnico di Torino, from September 2017 to September 2018. He is currently an Assistant Professor with the University of Science and Technology Beijing. His research interests include modeling, optimization, and the control of vehicle and marine powertrains, and hydrogen production and safety.

JU LONGYU received the Ph.D. degree from the School of Automotive and Traffic Engineering, Jiangsu University, in 2016.

From 2020 to 2022, he was a Postdoctoral Researcher with the School of Vehicle and Mobility, Tsinghua University, where he focused on the development of active torsional vibration offsetting technology in range-extender vehicles. He is currently the Manager of the NVH Center, Jing-Jin Electric Technologies Company Ltd., developing a noise and vibration reduction method for NEV.

YANG FUYUAN received the B.S. and M.S. degrees in internal combustion engine engineering and the Ph.D. degree from Tsinghua University, Beijing, China, in 1990, 1994, and 2005, respectively. He is currently a Professor and the Deputy Head in education with the Department of Automotive Engineering, Tsinghua University. His research interests include advanced diesel engine, hybrid powertrain systems, and intelligent electric vehicle charging.